UC Berkeley
Postprints from CPL

Title
Forced forward smoldering experiments in microgravity

Permalink
https://escholarship.org/uc/item/5cg7f8hv

Journal
Experimental Thermal and Fluid Science, 28(7)

ISSN
0894-1777

Authors
Bar-Ilan, Amnon
Rein, Guillermo
Fernandez-Pello, A Carlos
et al.

Publication Date
2004-09-01

Peer reviewed

eScholarship.org Powered by the California Digital Library
University of California

FORCED FORWARD SMOLDERING EXPERIMENTS IN MICROGRAVITY

A. Bar-Ilan, G. Rein, A.C. Fernandez-Pello*

Department of Mechanical Engineering
University of California
Berkeley, CA 94720, USA

J.L. Torero

School of Engineering and Electronics
University of Edinburgh, Edinburgh EH9 3JN, UK

D.L. Urban

NASA Glenn Research Center
Cleveland, OH 44135, USA

Published in:
Experimental Thermal and Fluid Science, Vol. 28 (7), 2004, pp. 743-751.

* Corresponding author. Fax: (510) 642-6163, email: ferpello@me.berkeley.edu

ABSTRACT

Results from two forward forced-flow smolder tests on polyurethane foam using air as oxidizer conducted aboard the NASA Space Shuttle (STS-105 and STS-108 missions) are presented in this work. The two tests provide the only presently available forward smolder data in microgravity. A complimentary series of ground-based tests were also conducted to determine, by comparison with the microgravity data, the effect of gravity on the forward smolder propagation. The objective of the study is to provide a better understanding of the controlling mechanisms of smolder for the purpose of control and prevention, both in normal- and microgravity. The data consists of temperature histories from thermocouples placed at various axial locations along the fuel sample centerline, and of permeability histories obtained from ultrasonic transducer pairs also located at various axial positions in the fuel sample. A comparison of the tests conducted in normal- and microgravity indicates that smolder propagation velocities are higher in microgravity than in normal gravity, and that there is a greater tendency for a transition to flame in microgravity than in normal gravity. This is due primarily to the reduced heat losses in the microgravity environment, leading to increased char oxidation. This observation is confirmed through a simplified one-dimensional model of the forward smolder propagation. This finding has important implications from the point of view of fire safety in a space-based environment, since smolder can often occur in the forward mode and potentially lead to a smolder-initiated fire.

Keywords: Smoldering Combustion; Microgravity; Forward Forced Flow; Buoyancy Effects.

I. INTRODUCTION

Smoldering is a basic combustion problem that encompasses a number of fundamental processes, including: heat and mass transfer in porous media, endothermic pyrolysis of the combustible material, ignition, propagation and extinction of heterogeneous exothermic combustion reactions at the solid and gas pore interface [1,2]. Smoldering presents a serious fire risk because it is initiated at low temperatures and because the reaction can propagate slowly in the material interior and go undetected for long periods of time. It typically yields a substantially higher conversion of fuel to toxic compounds than does flaming (although at a lower rate), and may undergo a sudden transition to flaming. Smolder of cable insulation, another common fire hazard, is of particular concern in the space program; to date there have been a few minor incidents of overheated and charred cables and electrical components reported on Space Shuttle flights [3, 4]. Recently, with the establishment of the International Space Station, and the planning of a potential manned mission to Mars, there has been an increased interest in the study of smoldering in microgravity because of the need to preempt the possibility, and/or to minimize the effect of a smolder initiated fire during the operation of these facilities [3, 4].

There are two distinct classifications for one-dimensional propagation of a smolder reaction: opposed and forward [1,2]. These are defined according to the direction in which the fuel and oxidizer enter the reaction zone. In forward smolder, the mode reported here, the reaction front propagates in the same direction as the oxidizer flow. The heat released by the heterogeneous oxidation (smolder) reaction is transferred ahead of the reaction by conduction, convection, and radiation, heating the unreacted fuel. The resulting increase of the virgin fuel temperature leads to the onset of the smolder reaction, and consequently gives way to its propagation through the fuel. In smolder propagation, the combustion process is generally oxygen deficient, and the propagating reaction leaves behind a char that contains a significant amount of unburned fuel [1].

The rate of smolder propagation is dictated primarily by a balance between the rate of heat released by the reaction and the energy required to heat the solid fuel and gaseous oxidizer to the smolder reaction temperature. Increasing the oxidizer flow rate increases the rates of fuel oxidation and heat release, and consequently the rate of smolder propagation.

The aim of the Microgravity Smoldering Combustion (MSC) experiment is to provide a better fundamental understanding of the controlling mechanisms of smoldering combustion of porous materials under normal gravity and microgravity conditions. This in turn will aid in the prevention and control of smolder-originated fires, both on earth and in spacecrafts. The microgravity smoldering experiments have to be conducted in a space-based facility because smoldering is a very slow process and consequently its study in a microgravity environment requires extended periods of time. The microgravity experiments reported here, were conducted on board the NASA Space Shuttle. The most recent tests were conducted during the STS-105 (August 2001) and STS-108 (December 2001) missions; two forward forced flow tests with air as oxidizer. The MSC data are compared with normal-gravity data to determine the effect of gravity on smolder. The normal gravity experiments were conducted under exactly the same conditions as the microgravity experiments using the MSC apparatus.

II. FLIGHT HARDWARE

MSC tests were performed in a 21.7 liter, semi-cylindrical, hermetically sealed, aluminum combustion chamber (Fig.1, middle). The fuel sample, located in the chamber, consists of a

polyurethane foam cylinder, 132 mm diameter by 140 mm long, held in a 120 mm diameter sheath made out of Vespel to permit ultrasonic imaging of the progress of the smolder reaction. The sample diameter allows for a 10% compression of the fuel sample that prevents preferential oxidizer flow between the outer edge of the sample and the walls of the sheath. A schematic of the MSC flight hardware is shown in Fig. 1. The sample holder (Fig.1, bottom) consists of a Vespel sheath, a cylindrical disc igniter (an electrically heated wire, sandwiched between two porous ceramic discs) placed in contact with the interior end of the foam cylinder, a cylindrical metal housing for a char cylinder (120 mm diameter by 52 mm long) placed at the other side of the igniter, and aluminum support brackets. For these tests, a cap with the oxidizer flow inlet is fitted at the igniter end of the sheath, such that the oxidizer flows in the direction of smolder propagation. The oxidizer supply system provides a constant oxidizer mass flow through the foam sample via regulated pressure upstream of a choked flow orifice. The fuel sample is instrumented with an array of 9 thermocouples which provide an axial and a radial temperature history of the smolder propagation. The temperature data are later used to determine the rate of smolder propagation, and the characteristics of the reaction.

In addition to the thermocouples, a novel technique has been developed and applied to image the interior of the reaction by use of ultrasonic pulses as described by Tse et al. [6]. A set of 5 ultrasonic speaker/microphone transducer pairs are fixed lengthwise along the centerline of the sample to obtain line-of-sight average permeability data. The first speaker microphone pair is located 20 mm from the surface of the igniter, the second pair is 35 mm from the first and the remaining transducer pairs are spaced at 20 mm increments. The speakers and microphones are placed in an aluminum housing with the transducers sealed against circular openings in the housing. The housing is sealed against the side of the sheath, thereby allowing no flow leakage through the openings created by the transducers, and also insuring direct contact between the transducers and the foam sample. The openings for the transducers are covered in a fine copper mesh screen which does not interfere with the passage of the ultrasonic signal, and provides a conductive cooling effect for the transducer drums. Experiments show that a temperature rise of 50°C in the speaker drums is accompanied by a significant decrease in response.

All speakers are driven simultaneously, emitting a 40 kHz wave-train pulse consisting of six cycles, with a 150 V peak-to-peak amplitude after amplification. The microphones receiving the signal are selected by which data point is desired. The ultrasound imaging system (UIS) allows for monitoring of the smolder reaction because the attenuation of the ultrasound signal is proportional to the inverse square root of the permeability. It is observed that the passage of a smolder front leaves behind a char of significantly higher permeability than the unburned foam. Thus by monitoring changes in permeability, the UIS is able to image the location and velocity of the smolder front. The signal must be corrected appropriately for gas temperature, composition and pressure to obtain accurate measurement of the permeability of the foam.

The overall assembly integrates into a Get Away Special Canister or GAS-CAN (Fig.1, top) which is flown in the Shuttle cargo bay. The experiment operations are started by the crew or by the MSC computer via a time default. The smolder process is initiated in one fuel sample at a time. For the flow test cases, the oxidizer flow is initiated just prior to the igniter being switched on. Once the smolder front is established in the one fuel sample as determined by the temperature profile, ignition of the other fuel sample is started. Pressure, temperature and ultrasound data are recorded for each fuel sample once ignition is initiated. Data recording continues for two hours for each of the two fuel samples. Gases and remaining char samples from the tests are stored inside the chamber until removal post-flight.

III. RESULTS

The forward flow smolder experiments of the STS-105 and STS-108 Space-Shuttle missions were conducted with a forced oxidizer flow velocity of 3 mm/s and 5 mm/s respectively. In all experiments the oxidizer used is air. For the forced flow forward microgravity experiments, the ignition is achieved by supplying a constant heat flux at the igniter end of the sample for 400 s, after which the igniter is switched off. The experiments investigate the dependence of the smolder propagation velocity along a polyurethane foam sample on the flow rate of an air flow in the direction of smolder propagation. Polyurethane foam was selected as fuel because it is representative of materials commonly used on both earth and spacecraft-based facilities, its material properties are well known, and it maintains its structural integrity upon smoldering. The experimental conditions represent a convective environment with velocities similar to those that can be expected from ventilation systems in space facilities.

The primary results of the tests are the smolder ignition conditions, propagation velocity, smolder reaction temperature, and smolder reaction permeability. The characteristics of the smolder ignition are determined from the igniter power data and the temperature histories provided by the thermocouples on the igniter and foam near the igniter. The thermocouples placed along the foam sample centerline provide information to calculate the propagation velocity of the smolder front, as well as determining the intensity of the smolder reaction by measuring peak temperature. The radial temperature profiles provide information about the one-dimensionality of the smolder propagation. The line-of-sight average permeability histories provided by the ultrasonic transducer pairs provide permeability data as well as a second non-intrusive measurement of the smolder propagation velocity. This work presents the first ultrasonic data obtained from a microgravity forward smoldering combustion experiment.

Because of resources limitations, only two microgravity forward-smolder experiments were conducted. Despite the reduced number of experiments, some quantitative data can be obtained. Results for the smolder propagation velocity and smolder reaction temperature from both the normal gravity and microgravity tests are presented in Table 1. The results are divided into regions I, II, and III corresponding to the region influenced by the igniter, the middle region of the sample, and the region dominated by end effects, respectively [5].

Temperature profiles along the foam centerline for the 3 mm/s forced air flow case are presented in Fig. 2(a) for the microgravity test and in Fig. 2(b) for the normal-gravity simulation. Temperature profiles for the 5 mm/s forced air flow case are presented in Fig. 3(a) for the microgravity test and in Fig. 3(b) for the normal gravity test. Permeability histories for the 3 mm/s forced air flow case are presented in Fig. 4(a) for the microgravity test and in Fig. 4(b) for the normal gravity test. Figures 5(a) and 5(b) show the permeability plots for the 5 mm/s experiments. Post-flight images of the foam samples from the forced forward microgravity tests are presented in Fig. 6(a) and (b) for 3 mm/s and 5 mm/s forced air flow respectively, showing cutouts of the foam samples with details of the char structure. Images of the char structure in normal gravity are not presented, since the reversal of the smolder propagation towards the end of the sample (discussed below) disrupts the char structure.

For the 3 mm/s microgravity case, it can be seen that as the foam heats up the temperature near the igniter (TC's 0,1) first increases, then reaches a plateau of about 400°C, which is characteristic of smoldering, and then the temperature of the char (left behind the smolder front) increases again. Thermocouple 2 follows the same pattern but does not reach as high of a temperature. This is indicative of upstream consumption of oxygen by the char oxidation.

This is further evidenced with thermocouple 3 that stabilizes at about 320°C. It has to be noted that 320°C is already a characteristic temperature for endothermic pyrolysis. The area of the foam corresponding to these 4 thermocouples corresponds to the first 55 mm of the sample. The heating period is mostly influenced by the igniter and it lasts 400 s. As the igniter is turned off a slight decrease in the temperature of the foam can be perceived. but it is followed past 500 s by a sudden generation of heat. Temperatures corresponding to the first 35 mm of the sample (TC 0-3) reach about 450°C, which is typical of char oxidation. The temperature increase is felt beyond this region (TC 4, 5) but seems to be mostly driven by the heat generated in the first 35 mm of the foam. A weak re-kindling of the reaction is observed on the temperature traces corresponding to thermocouples 5 and 6 (75 to 95 mm).

The temperature traces show a reaction first driven by the igniter and then controlled by energy supply from the char oxidation in the first 35 mm of the foam. Char oxidation consumes the oxygen available and the smoldering reaction fades favoring pyrolysis. Once the char close to the igniter is consumed and the temperature in this region decreases, oxygen flows again and heat generation can be observed once more between 75 and 95 mm. The reaction is not strong enough to progress through the pyrolyzed fuel and eventually extinguishes at a distance more than 35 mm away from the sample end.

Figure 4(a) shows a dramatic increase in permeability that coincides in location with the regions in the char where the temperature reached the highest value. Figure 6(a) is a photograph of a cross-section of the sample. It can be clearly observed that in the region close to the igniter the char is almost completely consumed. This coincides well with the temperature histories that show strong char oxidation activity. The re-kindling of the reaction between 75 and 95 mm is also present as an area where the char shows large voids. Finally, a transition zone between the char and the unburned foam can be observed between thermocouples 6 and 7. This transition region is characterized by pyrolyzed foam. This thick region of degraded foam is typically observed for extinction conditions. It is important to note that the extinction region covers the entire sample cross section. The importance of this observation will be clearer later when the 5 mm/s flow condition is discussed.

The 3 mm/s normal-gravity case in Fig. 2(b) shows a completely different behavior. The temperature increases due to the igniter and the first thermocouples (TC 0, 1) reach the same plateau at approximately 400°C. It is important to note that the temperature increase is slower than in microgravity, indicating larger heat losses. Once the plateau is reached the temperature immediately begins to decrease, contrary to the behavior in microgravity. What follows is a succession of thermocouple traces that reach a decaying maximum value and then cool down rapidly. Peak temperatures, although decaying, remain within ranges typical of smoldering. Char oxidation has no significant impact on the temperature traces. Nevertheless, the char oxidation reaction is clearly present since the peak temperature is slowly decreasing.

After 1000 s the reaction is about 35 mm away from the end of the sample and a gradual increase in the reaction rate throughout the entire foam follows. This effect has been previously described and is related to the decrease in pressure drop through the foam that allows an increase in the total contribution of buoyancy to the supply of oxidizer. At time greater than 1300 s a secondary opposed smolder reaction through the char follows.

The evolution of the permeability follows a similar trend to that of the temperature histories. A consistent increase in permeability is observed and at each stage of the propagation the change in permeability is smaller. Past 1000 s the increase in permeability continues showing peaks at the locations of the secondary opposed smolder reaction.

From the above description it is seen that comparison of both sets of temperature histories (Figures 3(a) and 3(b)) shows an important difference between microgravity and normal-

gravity experiments. In microgravity the flow through the char is restricted to that of the forced flow, this flow is unable to cool down the char and char oxidation is favored close to the igniter. The result, as previously mentioned, is a reaction front dominated by char oxidation. In normal gravity, buoyantly induced re-circulation flows within the char and external natural convection result in rapid cooling of this region. This precludes char oxidation and allows a smolder front to propagate across the sample. Heat generation from the smolder reaction is much weaker than that from char oxidation, so propagation is slower. Furthermore, radial heat losses are enhanced by buoyancy so the net heat input to the virgin foam is weaker forcing a slower propagation. It is important to note that despite the fact of having a weaker smolder front that propagates slower in normal gravity, the reaction manages to progress through the entire sample. In micro-gravity, the consumption of oxygen next to the igniter favors pyrolysis and leads to premature extinction.

In the 5 mm/s case, the first thermocouples (TC 0, 1) are seen to ramp up to approximately 450°C at 450 s typical of the onset of a smolder reaction, at which point the igniter is switched off. After a short plateau, the temperatures at TC 0, 1 continue to climb until reaching a peak of greater than 500°C at approximately 600 s. It should be noted that noise in the signals of thermocouples 0, 1 create a gap in their histories between approximately 600-650 s. Thermocouple 2 follows a very similar trend, reaching 400°C approximately 50 s after the igniter thermocouples, and peaking at 500°C at the same time as the igniter thermocouples. The lower temperature of thermocouple 2 indicates that the char oxidation in the region near the igniter is consuming the oxygen supply downstream. However the increased oxygen supply of this test relative to the 3 mm/s microgravity test provides enough oxygen to continue the char oxidation in the region of thermocouple 2. This char oxidation reaction is carried further to thermocouple 3, which reaches a plateau at approximately 380°C and continues to increase in temperature to a peak of approximately 460ºC. In this case, the char oxidation region extends to thermocouple 4 as well. Thermocouple 4 shows a brief plateau at 300°C at 500 s, and then continues to increase to a peak of 400 ºC at 600 s, when the char oxidation reaction is peaking at all thermocouples 0-4.

The char oxidation reaction at thermocouple 4 is substantially weaker than at the location of the previous thermocouples and marks the transition to a region in which oxygen consumption from the secondary char oxidation is preventing the continued smolder propagation. Thermocouple 5 is observed to peak at only 375°C, and is responding primarily to the thermal wave from the char oxidation. However, unlike the 3 mm/s microgravity case, the 5 mm/s case shows a vigorous re-kindled smolder reaction further along the sample that begins at approximately 600 s and continues until reaching the end of the sample at 750 s. The increase in temperature of thermocouples 6, 7, at an axial position between 95 to 115 mm, is indicative of a smolder propagation continuing through the sample past the char oxidation region. The temperature histories of thermocouples 6, 7 both show multiple peaks after the first smolder front passage. Temperature at thermocouple 6 peaks twice at 375°C and then again at 395°C, and that of thermocouple 7 peaks twice at 360°C and then again at 410°C. This is indicative of further secondary char oxidation occurring in the continued smolder propagation region (95 to 115 mm). The heat generation from the secondary char oxidation at the location of thermocouple 7 drives a third temperature-peak in thermocouple 6 and a temperature rise in thermocouple 8. The temperature rise of thermocouple 8 is weaker than that of thermocouples 6, 7, and peaks at only 325°C. This marks the extinction of the reaction at the end of the sample. The char image of Fig. 6(b) shows that the reaction extinguishes near the end of the sample. The conical shape of the smolder front near the end of the sample indicates that radial heat losses are dominant in this region as the reaction is maintained only in

the central core of the fuel sample. The heat generated from the smolder reaction and the secondary char oxidation upstream is insufficient for further propagation of the smolder front, or for a reversal at the end of the sample. It needs to be noted that extinction for the 5 mm/s case differs from the 3 mm/s one where progression towards endothermic pyrolysis leads to extinction and heat losses are not the limiting process.

The permeability histories agree with the temperature histories. In Fig. 4(a) the first ultrasonic transducer pair at 25 mm displays a sharp increase in permeability corresponding to the time of the strong secondary char oxidation reaction occurring in the 0 to 55 mm region, as shown by the sharp temperature increases in thermocouples 0-4. Furthermore, the permeability history of the fourth transducer pair, at 100 mm, shows a secondary spike corresponding to the location and time of the re-kindled smolder and secondary char oxidation reactions at that position. The fifth transducer pair displays a much weaker permeability rise, corresponding to the extinction of the reaction at the end of the sample. Observations of the char images of Fig. 6(b) also correlate with the permeability and temperature histories. Although the region near the igniter (0 to 55 mm) in Fig. 6(b) does not show large voids, an end-on view of the char (figure not included here) shows a large void where the char has been almost entirely consumed. The transition region corresponding to 65 to 95 mm shows a more uniform denser char, indicating a weaker reaction in this region. Finally, the region of the re-kindled smolder reaction shows an area of char typical of a smolder reaction.

Thus similar to the 3 mm/s microgravity case, the 5 mm/s microgravity case shows a reaction first controlled by the igniter but leading quickly to a strong secondary char oxidation. This secondary char oxidation reduces the oxygen supply, but does not completely consumed it, allowing for a much larger region of secondary char oxidation. Once this secondary char oxidation has consumed the available fuel, the oxygen supply is able to reach further downstream positions. However, the reaction does not extinguish like in the 3 mm/s case, because the supply of oxygen is greater in this case, and stimulates a strong rekindling of the smolder reaction which is able to propagate through to the end of the sample.

The 5 mm/s normal-gravity case is very similar to the 3 mm/s normal-gravity case discussed above. Once ignition is achieved, the char immediately cools down due to increased buoyancy-induced heat losses. This permits the oxygen supply to reach the unreacted foam ahead of the igniter and propagate a smolder reaction through to the end of the sample. A comparison of Fig. 2(b) and Fig. 3(b) shows very similar temperature histories, however the 5 mm/s case has a faster propagation velocity. The temperature of thermocouple 7 in Fig. 3(b) reaches a peak at approximately 1000 s, whereas that of the same thermocouple in Fig. 2(b) only peaks at approximately 1500 s. This is due to the increased forced air flow rate in the case of the 5 mm/s normal-gravity test, which drives a greater heat release rate and hence a faster smolder propagation rate. Peak temperatures are only slightly higher in the case of the 5 mm/s normal-gravity test, as compared to the 3 mm/s normal-gravity case. It can be seen however that the reversal of the reaction at the end of the sample is characterized by higher temperatures in the 5 mm/s normal-gravity case than in the 3 mm/s normal-gravity case. This is again a function of the increased oxygen supply to the reaction, which under oxygen-limited conditions allows for a greater heat release. Permeability histories in Fig. 4(b) and Fig. 5(b) are very similar in the two normal-gravity cases. The 5 mm/s normal-gravity test shows a relatively steady increase in permeability marking the arrival of the smolder front at each ultrasonic transducer pair. The only substantive difference between the two normal-gravity permeability histories is the time scale.

From all these results it can be concluded that a comparison between the temperature profiles in microgravity and in normal gravity shows that the char temperature histories are

significantly different between the two conditions. In microgravity, the reduced heat losses leads to a hotter char, capable of sustaining a secondary char oxidation reaction but suppressing the smolder reaction through the consumption of the oxygen supply. In the low flow rate microgravity test, the subsequent smolder reaction is extinguished before propagating through the sample, whereas in the high flow rate microgravity test the increased oxygen supply is sufficient to sustain a smolder propagation through the entire sample. The normal-gravity tests display a markedly different behavior. The increased heat losses in normal-gravity force cooling of the char, which allows the forced air flow to pass through the char without major consumption of the oxygen. This permits the smolder reaction to be sustained and propagate (albeit more slowly than in the microgravity case) through the entire sample length at both low and high forced air flow rates.

IV. SIMPLIFIED THEORETICAL ANALYSIS

Smolder often occurs under oxygen-limited conditions [1], and consequently, the rate of heat release from the smolder reaction is directly proportional to the oxidizer mass flux. Away from extinction conditions, the smolder propagation velocity is then proportional to the heat release rate minus heat losses to the environment [5]. A one-dimensional model of smolder propagation is used to obtain an explicit expression for the smolder velocity and to correlate the experimental results. The model used in this study is based on the analysis of Dosanjh et al. [7] but extended to include the radial heat losses to the environment.

The model assumes a two-step chemical reaction consisting of an endothermic pyrolysis, followed by a combined smolder/oxidative-char reactions. The propagation rates of these two reactions have been shown to be slightly different in the forward smolder configuration, but for simplicity it is assumed that they are equal. The model also assumes that all of the oxidizer is consumed at the reaction. Thus the heat released is the product of the oxidizer mass flux and the heat of smolder combustion (per unit mass of oxidizer). Similarly, it is assumed that all the solid is pyrolyzed to char, thus the heat absorbed by the foam pyrolysis is the product of the mass flux of the solid fuel and the heat of pyrolysis (per unit mass of fuel). The resulting expression for the smolder velocity is [5]:

$$u_{sml} = \frac{Y_{O2,a}\rho_g u_g Q_{sml} - \dot{Q}''_{loss}\,{}^{A_L}\!/_{A_C}}{\left[(1-\phi)\rho_s c_{p,s} + \phi\rho_g c_{p,g}\right](T_S - T_a) - (1-\phi)\rho_s Q_P + Y_{O2,a}\rho_g Q_{sml}} \qquad (1)$$

Properties and parameters used in the calculations are shown in Table 2. Values for smolder temperature are taken from the experimental results and described in Table 1. Radial heat losses from the reaction zone to the environment were analytically calculated previously [8] to be 100 W/m^2 in microgravity and 700 W/m^2 in normal gravity, the difference being due to the buoyancy-driven heat losses in normal gravity. Values for the heat of smolder combustion and heat of pyrolysis are selected to optimize the comparison of the theoretical and experimental data. These values are shown and compared to other values in the literature in Table 3. These results are similar to those of Torero et al. [9] and Walther et al. [10], although since they did not take in account the radial heat losses, the values reported here are considered to be more accurate.

A comparison of predicted and measured smolder propagation velocities in microgravity and in upward normal-gravity are presented in Fig. 7. It is seen that the analysis predicts correctly the influence of the air flow on the smolder velocity in microgravity. In normal

gravity conditions, the model over-predicts the smolder propagation velocity for 5 mm/s. This seems to be due to a stronger char oxidation in this case, not predicted by the model, which does not consider buoyant flow on the total mass flux of oxidizer[9].

V. CONCLUSIONS

The present experiments, although limited, are unique in that they provide the only available information about forward smolder combustion in microgravity in sample-sizes large enough to allow the self-propagation of the smolder reaction. The experimental results provide further verification about the smolder controlling mechanisms and distinctive data for model verification.

A comparison of the tests conducted in normal gravity and microgravity indicates that heat losses in the char region behind the smolder front are an important controlling mechanism in the smolder propagation. In microgravity, reduced heat losses lead to a hotter char region which supports secondary char oxidation and either causes an extinction of the smolder reaction (low oxidizer mass flux) or a subsequent acceleration of the smolder propagation (high oxidizer mass flux). In normal gravity, the buoyancy-induced heat losses cause the char to cool rapidly, preventing a secondary char oxidation reaction but allowing for smolder propagation to occur throughout the sample length. This has been verified through analysis of the temperature and permeability histories as well as observation of the char structure from post-flight data.

A simplified theoretical analysis of the smolder propagation is used to correlate predicted smolder propagation velocities with experimentally measured values. The analysis predicts well the smoldering propagation velocities in microgravity but in normal gravity the agreement is only qualitative. The limitations of the simplified analysis necessitate a thorough examination of the effect of buoyancy flows, and the energy released and oxygen consumption from the char oxidation reaction. Examination of these effects, as well as the development of a numerical model, are ongoing.

Finally, it should be emphasized that the present conclusions are based on only two microgravity tests. Thus, these results cannot be generalized until further tests are conducted.

ACKNOWLEDGEMENTS

This work was supported by the National Aeronautics and Space Administration under grant NAG3-2026. The authors would like to acknowledge the comments and technical support of Dr. H.D. Ross, Franklin Vergili, the entire NASA Glenn engineering team and Ms. Sonia Fereres during the development of this work.

REFERENCES

1. Ohlemiller, T.J., Modeling of Smoldering Combustion Propagation, *Progress in Energy and Combustion Science*, Vol. 11 (1985), pp. 277-310.

2. T'ien, J.S., Shih, H.Y., Jiang, C.B., Ross, H.D., Miller, J., Fernandez-Pello, A. C., Torero, J.L. and Walther, D., Chap. 5, p.299-345, Microgravity Combustion: Fire in Free Fall, Ross, H. (ed.), Academic Press (2001).

3. Ross, H.D., *National Fire Protection Association*. Annual Meeting, May (1996).

4. Friedman, R., Risk and Issues in Fire Safety on The Space Station, *NASA* Technical Memorandum 106403 (1994).

5. Torero, J.L., Fernandez-Pello, A.C. and. Kitano, M., Opposed Forced Flow Smoldering of Polyurethane Foam, *Combustion Science and Technology*, Vol. 91, No. 1-3 (1993) pp. 95-117.

6. Tse, S.D., Anthenien, R.A., Fernandez-Pello, A.C. and Miyasaka, K., An Application of Ultrasound Tomographic Imaging to Study Smoldering Combustion, *Combustion and Flame*, Vol. 116, No. 12 (1998), pp.120-135.

7. Dosanjh, S.S. and Pagni P.J., Forced Counter-current Smoldering Combustion, *The ASME-JSME Thermal Engineering Joint Conference*, Honolulu, Hawaii, Vol 1 (1987), pp. 165-173.

8. Bar-Ilan, A., Rein, G., Fernandez-Pello, A.C., Torero, J.L. and Urban, D.L., "The Effect of Buoyancy on Opposed Smoldering", *Combustion Science and Technology* (submitted for publication) (2003).

9. Torero, J.L. and Fernandez-Pello, A.C., Forward Smolder of Polyurethane Foam in a Forced Air Flow**,** *Combustion and Flame,* Vol. 106, No. 1-2 (1996), pp. 89-109.

10. Walther, D.C., Fernandez-Pello, A.C. and Urban, D.L., Space Shuttle Based Microgravity Smoldering Combustion Experiments, *Combustion and Flame* Vol. 116, No. 3 (1998), pp. 398-414.

NOMENCLATURE

Symbol	Definition
A_L/A_c	Lateral to cross-sectional areas ratio for the smolder front
$c_{p,s}$	Specific heat of the solid
$c_{p,g}$	Specific heat of the gas
$\dot{Q}''_{loss}$	Radial heat-loss flux to the exterior
Q_{sml}	Heat of smoldering
Q_p	Heat of pyrolysis
T_a	Ambient temperature
T_S	Temperature of smolder
u_g	Gas velocity
u_{sml}	Smolder front propagation velocity
Y_{O2}	Mass fraction of oxygen

Greek symbols

f	Porosity of the foam
ρ_s	Density of the solid
ρ_g	Density of the gas

Subscripts

a	Ambient conditions
g	Gas
p	Pyrolysis
s	Solid
sml	smolder

TABLE CAPTIONS

Table 1. Smolder propagation velocities and smolder temperatures from normal and microgravity experiments.

Table 2. Properties and parameters used in the calculations

Table 3. Values for the heat of smoldering and heat of pyrolysis

FIGURE CAPTIONS

Figure 1. MSC flight assembly. At top is the overall assembly, at middle is the chamber and at the bottom is the sample holder.

Figure 2. Thermocouple histories for forced air velocity of (a) 3 mm/s for microgravity, (b) 3 mm/s for normal gravity.

Figure 3. Thermocouple histories for forced air velocity of (a) 5 mm/s for microgravity and (b) 5 mm/s for normal gravity.

Figure 4. UIS permeability histories for forced air velocity of (a) 3 mm/s for microgravity, (b) 3 mm/s for normal gravity.

Figure 5. UIS permeability histories for forced air velocity of (a) 5 mm/s for microgravity and (b) 5 mm/s for normal gravity.

Figure 6. Post-flight image of foam sample cutout showing char for forced air velocity of (a) 3 mm/s in microgravity, and (b) 5 mm/s in microgravity.

Figure 7. Predicted and measured smolder propagation velocity as a function of inlet air velocities.

TABLES

Forced Air Velocity [mm/s]	Smolder Velocity [mm/s]						Smolder Temperature [°C]					
	Region I		Region II		Region III		Region I		Region II		Region III	
	0g	*1g*	*0g*	*1g*	*0g*	*1g*	*0g*	*1g*	*0g*	*1g*	*0g*	*1g*
3	0.25	0.19	0.15	0.10	-	0.12	399	396	406	355	-	361
5	0.40	0.24	0.23	0.16	0.25	0.22	398	398	428	387	375	406

Table 1. Smolder propagation velocities and smolder temperatures from normal and microgravity experiments.

Quantity	Units	Value
T_a	[°C]	25
$c_{p,s}$	[kJ/kgK]	1.70
$c_{p,g}$	[kJ/kgK]	1.09
ρ_s	[kg/m^3]	1034
ρ_g	[kg/m^3]	1.225
Y_{O2}	-	0.23
ϕ	-	0.975
A_L/A_C	-	1.33

Table 2. Properties and parameters used in the calculations

[kJ/kg]	Q_{sml}	Q_P
This work	4550	337
Torero et al. [9]	3900	300
Walther et al. [10]	4550	-

Table 3. Values for the heat of smoldering and heat of pyrolysis

FIGURES

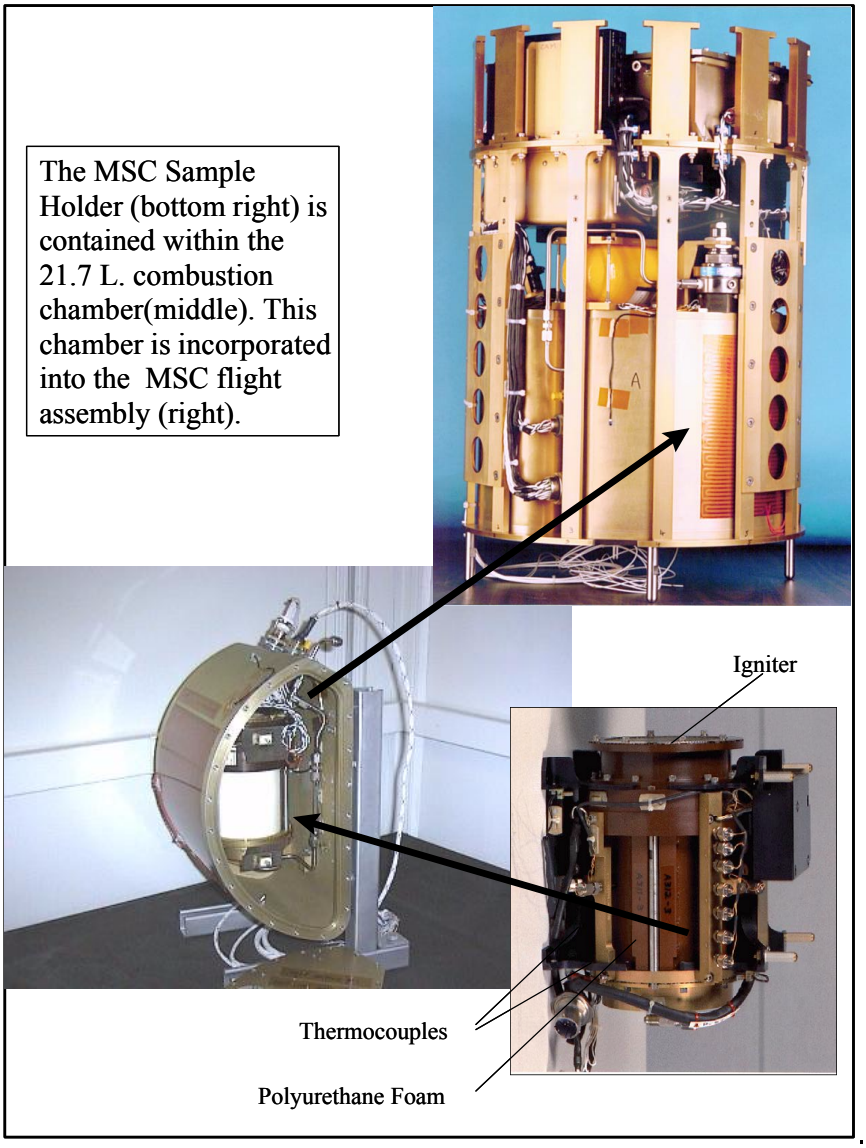

Figure 1. MSC flight assembly. At top is the overall assembly, at middle is the chamber and at the bottom is the sample holder.

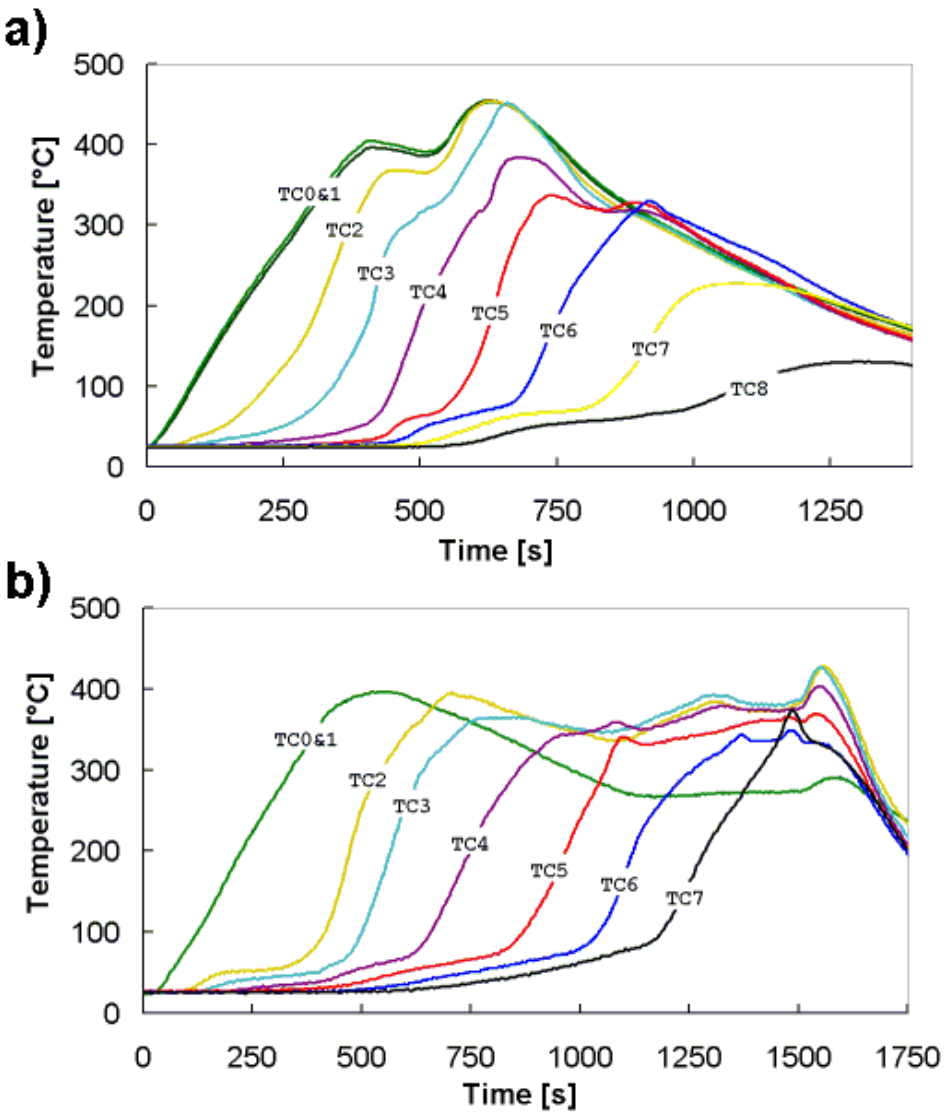

Figure 2. Thermocouple histories for forced air velocity of (a) 3 mm/s for microgravity, (b) 3 mm/s for normal gravity.

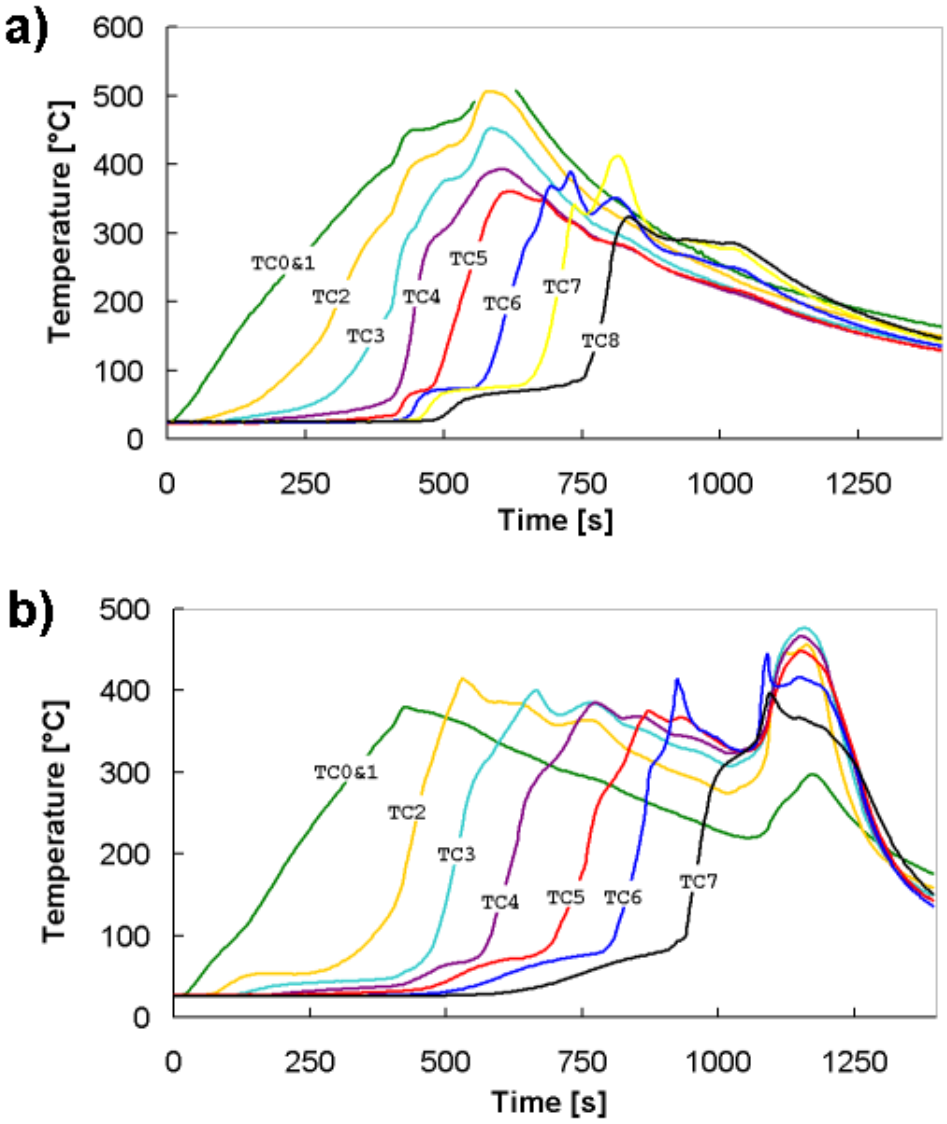

Figure 3. Thermocouple histories for forced air velocity of (a) 5 mm/s for microgravity and (b) 5 mm/s for normal gravity.

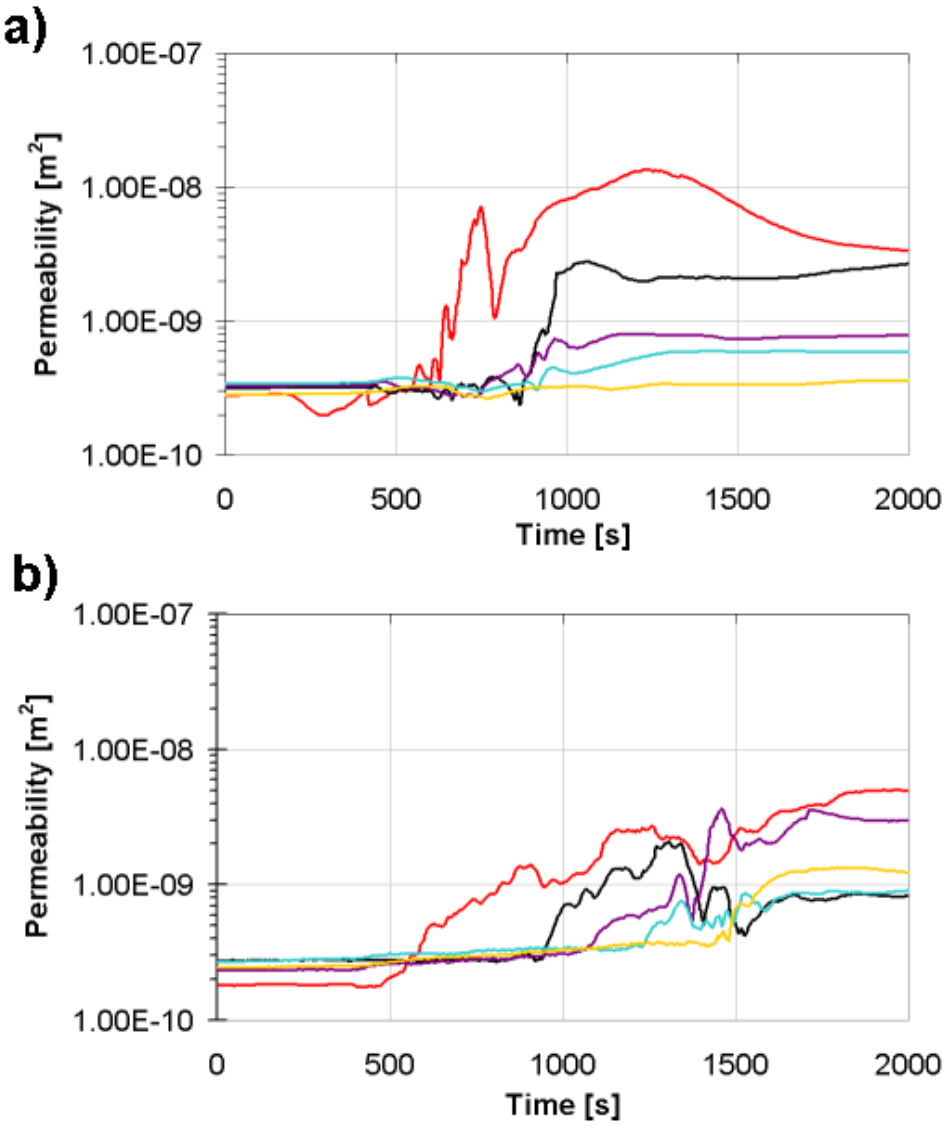

Figure 4. UIS permeability histories for forced air velocity of (a) 3 mm/s for microgravity, (b) 3 mm/s for normal gravity.

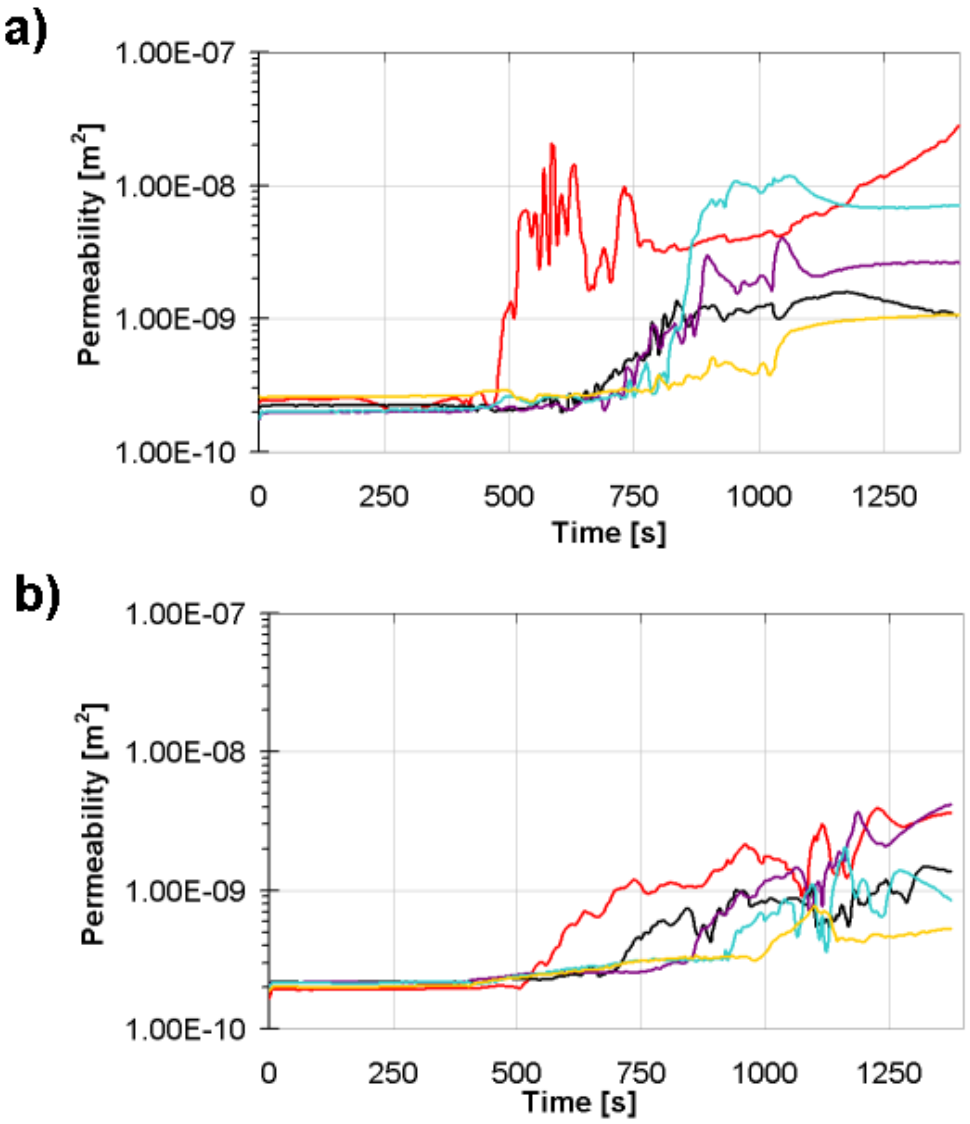

Figure 5. UIS permeability histories for forced air velocity of (a) 5 mm/s for microgravity and (b) 5 mm/s for normal gravity.

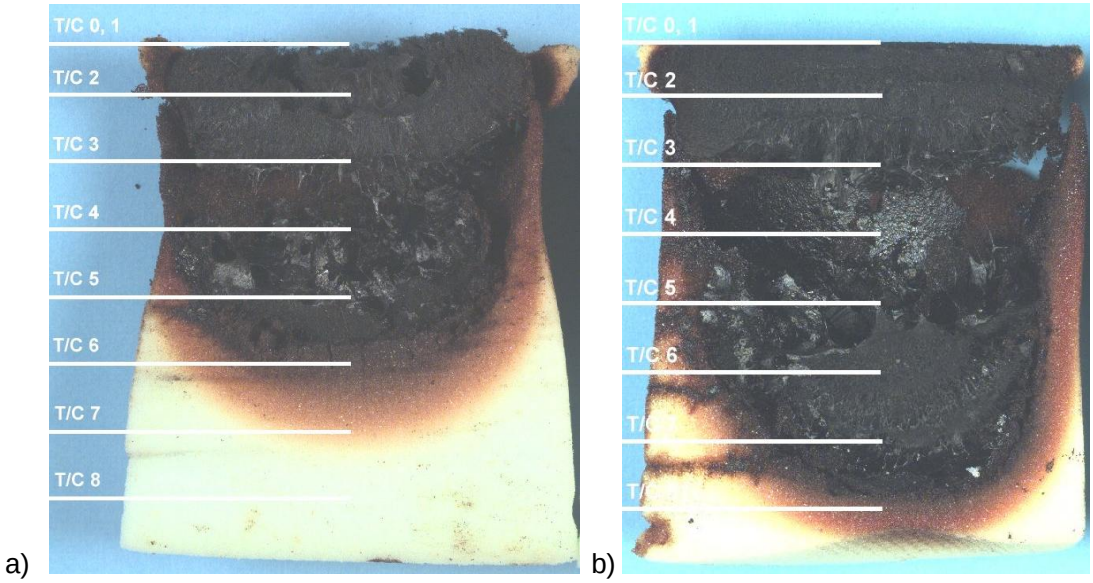

Figure 6. Post-flight image of foam sample cutout showing char for forced air velocity of (a) 3 mm/s in microgravity, and (b) 5 mm/s in microgravity.

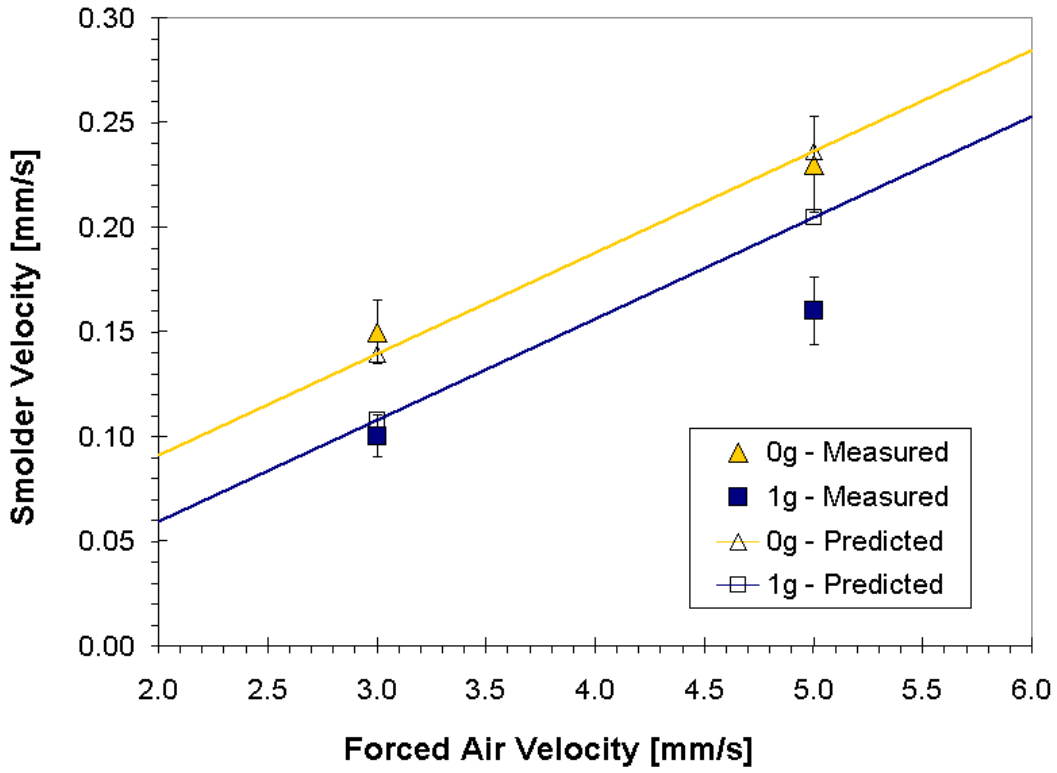

Figure 7. Predicted and measured smolder propagation velocity as a function of inlet air velocities.